CHAPTER 4

EQUIVALENT CIRCUIT MODELS USING CPE FOR IMPEDANCE SPECTROSCOPY OF ELECTRONIC CERAMICS

4.1 Introduction

Electronic ceramics are technological materials having vast variety of applications such as actuators and sensors, computer memories, electrically controlled microwave tuning devices for RADAR applications etc and are playing key role in electronics industry today [Moulson et al. (2003); Buchanan (2004); Sebastian (2008); Sebastian et al.(2017)]. In actual practice the ceramics are integrated to some other systems or components. A prior knowledge of an equivalent circuit suitable to represent their behavior in a given frequency range may greatly facilitate the overall optimum design of the systems. In the study of electrical behavior of ceramics impedance spectroscopy is being increasingly used which, in turn, is proving to be very useful for obtaining equivalent circuit models also **[**Macdonald et al. (2005); Jonscher (1983); Sinclair et al. (1994)]. In this technique, depending upon the possible charge transfer processes thought to be present in the material, suitable equivalent circuits are chosen to represent the electrical behavior by comparing the experimental plots with the simulated ones for various model circuits. Usually combinations of resistances (R) and capacitances (C) suffice for dielectrics, combinations of R and inductance L suffice for magnetic systems and combinations of R, L and C suffice for ferro/piezoelectrics **[**Macdonald et al. (2005); Jonscher (1983); Sinclair et al. (1994); Sinclair et al.(1989); Morrison et al. (2001); Irvine et al. (1990); Pandey et al. (1995); Katare et al. (1999); Katare et al. (1997); Chaitanya (2009); Chaitanya et al. (2014); Chaitanya et al. (2015);

Chaitanya et al. (2011); Pandey et al (1998); Maiti et al. (1986); Pandey et al (1997); Kumar et al. (2005), West et al.(1997)]. Sometimes it is found that the lumped - component - type of models do not yield good fits and their simulated patterns do not show even qualitative resemblance with the experimental plots. The situation is then rescued by assuming presence of distributed components and/or resorting to Constant Phase angle Elements (CPE) connected in a suitable way [Macdonald et al. (2005); Jonscher (1983); Abram et al. (2003)]. Large amount of literature on impedance spectroscopy of electronic ceramics is available where various types of models have been used. As the technique of impedance spectroscopy has expanded to diverse fields from electrochemistry to electronic ceramics to medical diagnostics etc. increasing use of variety of models involving CPE and other components and their interpretations is being witnessed [Raistrick et al. (2005); Pandey et al. (2017) and reference therein]. However, a clear cut recipe for inferring the presence of CPE, the way a CPE may be incorporated in the equivalent circuit model and the values of the parameters be estimated is not available.

In this chapter simulated complex plane plots of immittance functions viz impedance (Z), admittance (Y), electric modulus (M) and permittivity (ε) for some simple equivalent circuit models containing CPE are presented with a view to facilitate the choice of models involving CPE by comparing the experimental results with the simulated plots. The experimental data obtained for $Ba_{1-x}Sr_xTiO_3$ (x=0.35) ceramic system is analyzed and a model equivalent circuit involving CPE representing the data is developed. The values of the components are estimated and their accurate values are obtained by using complex non-linear least squares (CNLS) procedure [Macdonald (2005)]. In the next section general ideas of impedance spectroscopy and the most important features of models involving resistive, capacitive and inductive elements are

summarized for ready reference. This is followed by simulation of models involving CPE, analysis of the available experimental impedance data and conclusions.

4.2. General Ideas

A polycrystalline ceramic comprises a large number of small crystallites called grains joined in random crystallographic orientations. The inter-grain region, called the grain boundary has, because of its mismatch, strained bonds. Therefore, the properties of inter-grain regions are different from those of the bulk i.e. grains. This fact gives rise to some very interesting and useful properties which are exploited in commercial devices [Moulson et al (2003);]. In glass - ceramics the grain boundary consists of uncrystallized glassy matrix [Macmillan (1979); Kingery et al. (1976); Lewis (1989); Herczog (1973); Patridge (1991); Patridge (1994)]. Usually, it is the interplay of 'grain' and 'grain boundary' behavior that bestows ceramics with several technologically useful properties. The understanding and controlling of this interplay with the help of processing variables, additives, ingredients or reduction in grain size dwelling in nanometers range is the subject of intensive research activities at present. A ceramic material prepared in powder form or as a glass - ceramic is processed and fabricated in some shape to which usually suitable electrodes are connected for device applications. Thus the overall property of a ceramic sample would get contributions from grains, grain boundaries and electrode interfaces and an electronic ceramic component may be treated as a grain - grain boundary – electrode system. In order to get a reproducible behavior and to develop materials having desired properties these contributions must be separated out. The method of impedance spectroscopy or Complex Impedance Analysis has emerged as a very powerful tool for this purpose in recent years [Macdonald et al. (2005)].

The electrical behavior of a system can be expressed in terms of interrelated functions known as impedance ($Z^*=Z' - jZ''$), admittance ($Y^*= (Z^*)^{-1} = Y' + jY''$), permittivity ($\varepsilon^* = (j\omega C_0 Z^*)^{-1} = \varepsilon' - j\varepsilon''$) and modulus ($M^* = (\varepsilon^*)^{-1} = j\omega C_0 Z^* = M' + jM''$), where $j = \sqrt{-1}$, $\omega = 2\pi f$, f being the frequency of the AC excitations used in the measurement and C_0 is the capacitance of the empty cell used to house the sample [Macdonald et al. (2005)]. Due to specific relationship between these broadly termed immittance functions, they are suitably used to extract information about the components used in the equivalent circuit models and hence about the behavior of the system [Macdonald et al. (2005); Pandey et al. (2017) and reference therein; Kochowski et al. (2002)]. It has been reported that a study of the ceramic system based on the information conveyed by only one of these four functions does not suffice and two or more functions should be looked at [Macdoanld et al. (2005); Pandey et al. (1995); Katare (1997); Pandey et al. (1998) , West et al. (1997)].

For complex impedance analysis, the real and imaginary parts of the complex impedance ($Z^*=Z - jZ''$) are measured as a function of frequency. The values of Z' and Z'' are plotted as a function of frequency and also in the complex plane (i.e. Z'' vs Z'). The resulting plots are , in general, collectively called impedance spectra. The Z'' vs Z' plots are usually semicircular distorted/ overlapping arcs [Macdonald et al (2005); Jonscher (1983); Sinclair et al (1994); Pandey et al. (1995)]. These arcs are attributed to stem from various charge transfer processes thought to be present in the system, such as those in grains, grain boundaries and electrodes etc, that may be represented by suitable equivalent circuit models. As a parallel RC circuit possesses one time constant RC, this circuit model is generally used to represent one charge transfer / polarization process. A parallel RC circuit model is schematically shown in Figure 4.1 (a)

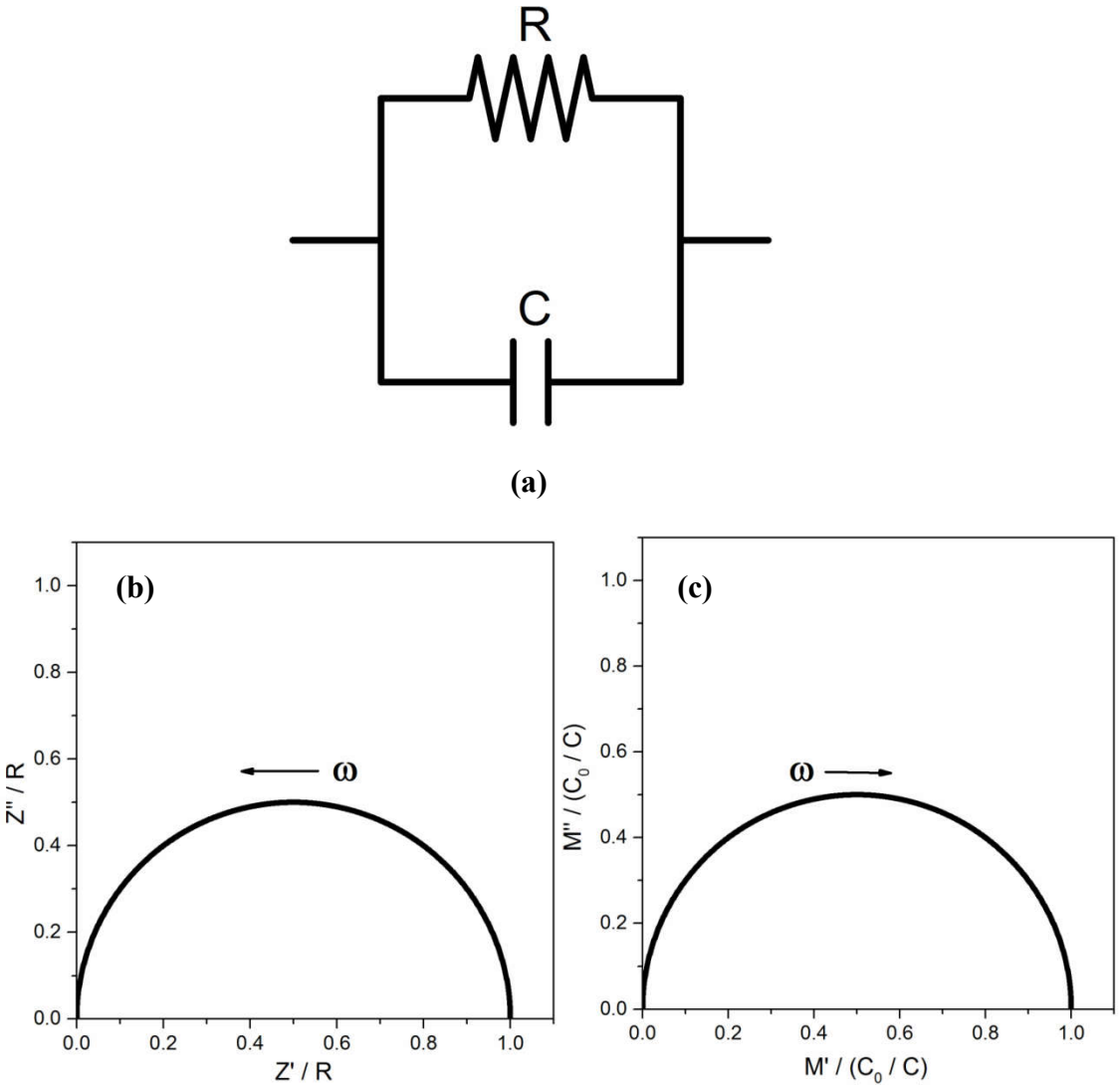

Figure 4.1: (a) A parallel RC equivalent circuit model, (b) Normalized plot of Z''/R vs. Z'/R, (c) Normalized plot of $M''/(C_0/C)$ vs. $M''/(C_0/C)$ for parallel RC circuit model

The various immittance functions for this model are given as [Macdonald et al. (2005); Pandey et al. (1995);]

$$Z'' = R\left(\frac{1}{1+\omega^2 C^2R^2}\right) \quad , \quad Z'' = R\left(\frac{\omega CR}{1+\omega^2 C^2R^2}\right) \tag{4.1}$$

$$Y' = \frac{1}{R} \quad , \quad Y'' = \omega C \tag{4.2}$$

$$M' = \frac{C_0}{C}\frac{\omega^2 C^2R^2}{1+\omega^2 C^2R^2} \quad , \quad M'' = \frac{C_0}{C}\frac{\omega CR}{1+\omega^2 C^2R^2} \tag{4.3}$$

$$\varepsilon' = \frac{C}{C_0} \quad , \quad \varepsilon'' = \frac{C}{C_0}\frac{1}{\omega CR} \tag{4.4}$$

The limiting values at $\omega \to 0$ and $\omega \to \infty$ are given below

$$Z'|_{\omega\to 0} = R \ , \ Z'|_{\omega\to\infty} = 0 \ , \ Z''|_{\omega\to 0} = 0 \ , \ Z''|_{\omega\to\infty} = 0 \tag{4.5}$$

$$Y'|_{\omega\to 0} = \frac{1}{R} \ , \ Y'|_{\omega\to\infty} = \frac{1}{R} \ , \ Y''|_{\omega\to 0} = 0 \ , \ Y''|_{\omega\to\infty} = \infty \tag{4.6}$$

$$M'|_{\omega\to 0} = 0 \ , \ M'|_{\omega\to\infty} = \frac{C_0}{C} \ , \ M''|_{\omega\to 0} = 0 \ , \ M''|_{\omega\to\infty} = 0 \tag{4.7}$$

$$\varepsilon'|_{\omega\to 0} = \frac{C}{C_0} \ , \ \varepsilon'|_{\omega\to\infty} = \frac{C}{C_0} \ , \ \varepsilon''|_{\omega\to 0} = \infty \ , \ \varepsilon''|_{\omega\to\infty} = 0 \tag{4.8}$$

Also Z' , Z" , M' , M" satisfy the following equations

$$(Z'-R/2)^2 + Z''^2 = (R/2)^2 \tag{4.9}$$

$$(M' - C_0/2C)^2 + M''^2 = (C_0/2C)^2 \tag{4.10}$$

which indicate that Z" vs Z' plot for this model circuit is a semicircular arc passing through the origin and has center at the point (R/2, 0). This arc intercepts the Z' axis at the point (R, 0) at the low frequency side and shows maximum value when $\omega RC = 1$. Thus values of R and C can be obtained by noting the low frequency intercept of the Z" vs Z' curve with the Z' axis and the value of frequency where Z" peaks. As indicated by Equation (4.10) the corresponding M" vs M' plot is also a semicircular arc passing through origin and having a high frequency intercept with the M' axis at C_0/C that too can be used for determining the value of C [Macdonald et al. (2005); Pandey et al. (1995)]. The Y" vs Y' and ε" vs ε' plots are vertical straight lines. A simple equivalent circuit model that could be used to represent two polarization/charge transfer processes such as sample-electrode system would have two parallel RC's connected in series. A

general practice is to choose one parallel RC circuit to represent one process and add further RC's in series to represent the other processes. Thus a simple equivalent circuit model for representing grain - grain boundary - electrode system may comprise three parallel RC's connected in series. Choice of a suitable model is a difficult process, becoming more so since several models can be found that show same behavior [Macdoanld et al. (2005); Pandey et al. (1995)]. However, attempts are made to choose a simple equivalent circuit model to start with. This is greatly facilitated by comparing the experimental plots with simulated ones and keeping in mind the charge transfer/polarization processes thought to be possibly present in the system.

Simulated immittance patterns for various models involving resistance (R), capacitance (C) inductance (L) are available in literature and have been used. In what follows some extremely useful hints for choosing a model to represent experimental results are summarized:

(i) Study of a ceramic system based on the information conveyed by only one of the four immittance functions might lead to erroneous conclusions and two or more functions viz. impedance (Z*) and modulus (M*) or admittance (Y*) and permittivity (ε *) should be looked at [Pandey et al. (1995); Chaitanya et al. (2015)].

(ii) Appearance of clear semicircular arc in both Z* and M* complex plane plots indicate that the experimental data may be modeled by a single parallel RC circuit [Macdonald et al. (2005); Pandey et al. (1995)].

(iii) A semicircle in Z" vs. Z' plot and a depressed looking arc in M" vs. M ' plot or vice -versa indicate that the model may comprise at least two parallel RC's (say R_1-C_1 and R_2-C_2) in series with ratios of time constants R_2C_2/R_1C_1, in the range 1 to 5 [Pandey et al. (1995)]. Appearance of two clear semicircular arcs indicates presence of two processes.

(iv) A semicircular arc with steeply rising branch (not a linear) at low frequency side in Z" vs Z ' plot and a shifted arc in the corresponding M" vs. M' plot indicates the presence of series C [Pandey et al. (1998)].

(v) A semicircular arc with steeply rising branch (not a linear) at high frequency side in M" vs. M' plot and a shifted arc in Z" vs Z' plot indicates the presence of series R in the equivalent circuit [Pandey et al. (1995)].

(vi) A semicircular arc with changed sign of Z" in the whole frequency range in Z " vs. Z ' plot points towards the possible presence of parallel R-L circuits [Katare et al. (1999)].

(vii) From an experimental Z" vs Z' plot showing a cross over from positive values of Z" to negative values or vice versa within the overall frequency range covered in the experiment, presence of all R, L and C is inferred [Macdonald et al. (2005); Chaitanya et al. (2014); Chaitanya et al. (2011)].

(viii) A linear portion in the Z" vs Z' or/and other immittance plots may indicate the presence of a series CPE in the model [Macdonald et al. (2005); Katare et al. (2003)]. A depressed semicircular immittance plot may indicate the presence of parallel CPE [Raistrick et al. (2005); Casciola et al. (1983)].

A glance at all the immittance plots of the experimental data obtained for different variables, such as composition and temperature, collectively together, and keeping in mind the hints listed above is found to be of great help in choosing a model [Chaitanya et al. (2011)]. Once the model has been chosen, the values of the components are estimated by comparing the experimental plots with the simulated ones. The values are determined more accurately by using these as initial guesses in a complex non-linear least square (CNLS) fitting procedure [Macdonald (2005); Pandey (1992)]. When the fittings are poor the model is modified keeping in mind the possibilities of processes

present/dormant, emerging or dominating in the system under study as the variables are altered. In the situations where two or more models seem physically feasible, that particular model is to be accepted which gives lowest value of the sum of squares of errors in the CNLS runs [Macdonald (2005)].

For usual dielectric materials models involving lumped resistive (R) and capacitive (C) components suffice where as for magnetic or piezoelectric materials inductive (L) elements are also included [Macdonald et al. (2005); Katare et al. (1999); Chaitanya (2009); Chaitanya (2011)]. For the cases where the experimental impedance data cannot be represented by equivalent circuit models based on lumped circuit elements (i.e. the CNLS does not show a good fit), presence of certain distributed elements or constant phase elements (CPE) is invoked. A CPE is a mathematical realization of a system in which the phase angle between applied ac voltage and resulting current remains independent of the frequency [Raistrick et al. (2005)]. There are various view points for the possible sources of such a behavior. However, larger consensus leans towards the belief that the CPE behavior arises due to presence of distribution in time constants in the material-electrode systems. This is one of the reasons for the widespread use of CPE in impedance spectroscopy [Macdonald et al. (2005); Orazem et al. (2013); Boukamp et al. (2004); Dissado et al. (1988); Hirschorn et al. (2010); Garcia et al. (2006)]. Therefore, when good fits are achieved by using models involving CPE, it is concluded that the system at hand possesses distribution in certain properties. The importance of a constant phase response was probably first emphasized by Fricke (1932). The CPE was explicitly mentioned by Cole et al. (1941) and its importance has been emphasized in recent times by Johnscher (1983) and Macdonald et al. (2005). Number of equivalent circuit models involving CPE are available in literature and ever increasing trend is being witnessed for the application of impedance spectroscopy in

diverse fields including agriculture and medical diagnostics by using CPE [Kochowski et al. (2002); Bao et al. (1992); Pandey et al. (2017) and references therein]. In the next section complex plane immittance plots of some simple models involving CPE are given that may be useful for selecting suitable models for representing experimental data. Their spectroscopic plots are not shown for brevity and only complex plane plots are shown.

4.3 Models

4.3.1 Model 1: Parallel combination of R and CPE

A parallel combination of resistance R and Constant Phase angle Element (CPE) is shown schematically in Figure 4.2(a). The impedance of a CPE is given as [Macdonald et al. (2005)]

$$Z_{CPE} = (Y_{CPE})^{-1} = [A_0(j\omega)^{\Psi}]^{-1} = \frac{1}{A_0\ \omega^{\Psi}} \cos\left(\frac{\Psi\pi}{2}\right) - j\ \frac{1}{A_0\ \omega^{\Psi}} \sin\left(\frac{\Psi\pi}{2}\right) \quad (4.11)$$

The Z'' vs Z' plot is a straight line with slope $\tan\left(\frac{\Psi\pi}{2}\right)$. For $\Psi = 0$, the imaginary part becomes zero and $Z_{CPE} = 1/A_0$ Ohms and the CPE behaves like an ideal resistor of value $1/A_0$. For $\Psi = 1$, the real part becomes zero and $Z_{CPE} = 1/(j\omega A_0)$ and the CPE behaves like an ideal capacitor of capacitance A_0 [Macdonald (2005)].

The expressions for real and imaginary parts of Y^* for the above model are given in Equation (4.12)

$$Y^* = 1/R + A_0 (j\omega)^{\Psi}\ ,\ \ Y' = \frac{1}{R} + A_0\ \omega^{\Psi} \cos\left(\frac{\Psi\pi}{2}\right)\ ,\ Y'' = A_0\ \omega^{\Psi} \sin\left(\frac{\Psi\pi}{2}\right)\ ) \quad (4.12)$$

It is seen that Y' and Y'' satisfy the equation

$$Y'' = Y' \tan\left(\frac{\Psi\pi}{2}\right) - \frac{1}{R}\tan\left(\frac{\Psi\pi}{2}\right) \quad (4.13)$$

which indicates that Y'' vs. Y' plot would be a straight line with intercept with Y' axis at the point (1/R,0) and slope equal to $\tan\left(\frac{\Psi\pi}{2}\right)$.

Also $$Z^* = \frac{R}{1+ A_0 R (j\omega)^{\Psi}} = \frac{R}{1+ (j\omega\tau)^{\Psi}} \quad (4.14)$$

where $\tau = (A_0 R)^{1/\Psi}$.

$$(Z' - \tfrac{R}{2})^2 + (Z'' + \tfrac{R}{2}\cot\tfrac{\Psi\pi}{2})^2 = (\tfrac{R}{2})^2(1 + \cot^2(\tfrac{\Psi\pi}{2})) \quad (4.15)$$

or ,

$$(Z' - \tfrac{R}{2})^2 + (Z'' + \tfrac{R}{2}\tan\theta)^2 = (\tfrac{R}{2})^2 (1 + \tan^2\theta) \quad (4.16)$$

which is the equation of a circle with center at $(\frac{R}{2}, -\frac{R}{2}\tan\theta)$ below the Z' axis and radius $(\frac{R}{2}\sqrt{1+\tan^2\theta})$. Here $\tan(\theta) = \cot\left(\frac{\psi\pi}{2}\right)$ ie $\Psi = 1-\theta/(\pi/2) = 1-\alpha$. This arc intercepts the Z' axis at the point (R , 0) at the low frequency side and θ is the angle between the Z' axis and the line joining the center of the arc to the origin. The corresponding values for M′, M″, ε′ and ε″ are obtained by using the relations for permittivity ($\varepsilon^* = (j\omega C_0 Z^*)^{-1} = \varepsilon' - j\varepsilon''$) and modulus ($M^* = (\varepsilon^*)^{-1} = j\omega C_0 Z^* = M' + jM''$) . The simulated immittance plots for this model are shown in Figures 4.2 (b-e) .The values have been suitably normalized for easy comparison. The values used for normalization are as under

$$Z' = R \text{ and } Y' = 1/R \text{ for } \omega = 0. \quad (4.17)$$

$$M' = C_0/A_0 \text{ and } \varepsilon' = A_0/C_0 \text{ for } \Psi = 1 \text{ and } \omega \to \infty \quad (4.18)$$

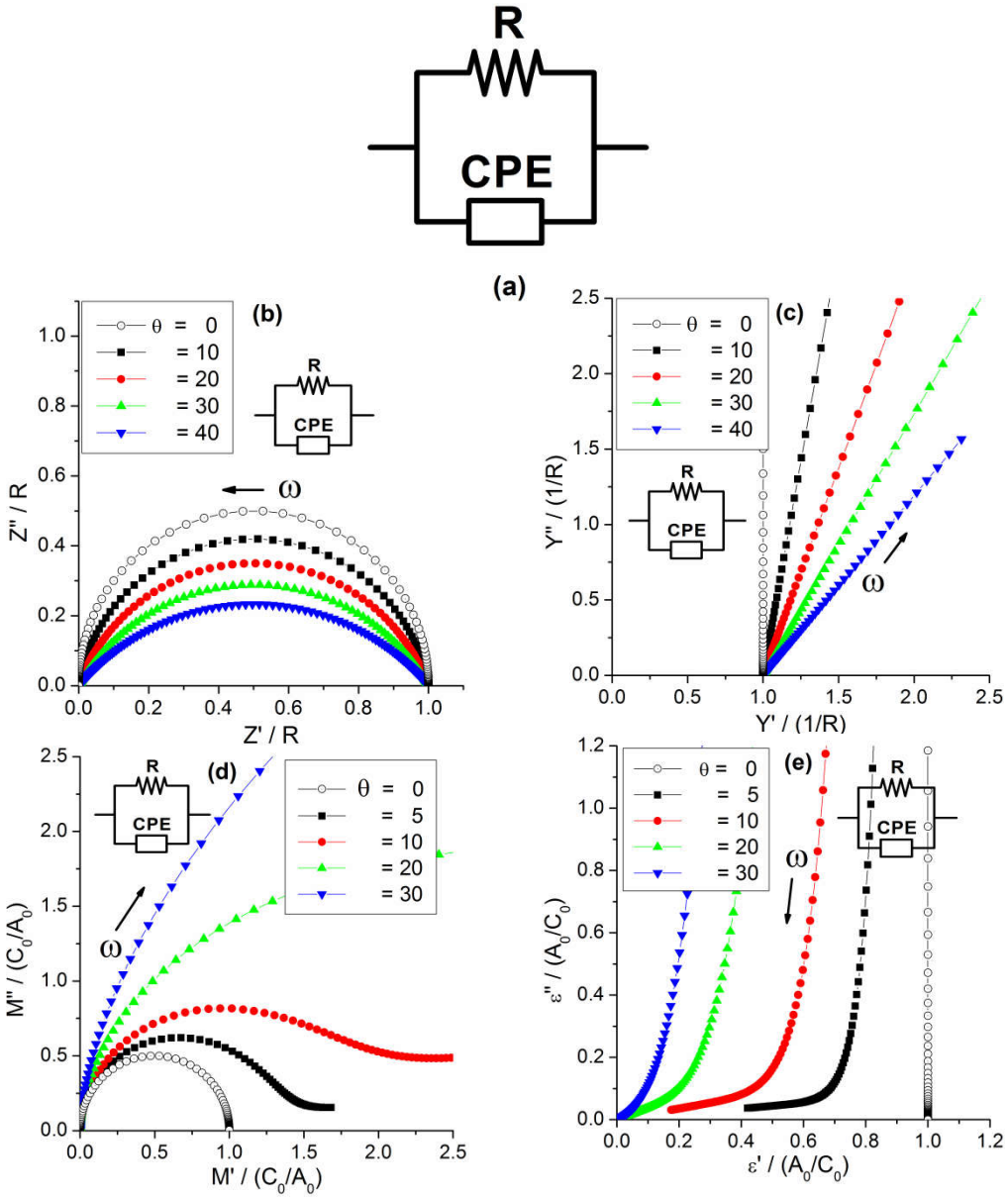

Figure 4.2: (a) Equivalent circuit model containing a parallel combination of resistance R and CPE (b) Plot of Z"/R vs Z'/R for various values of θ , where θ is the angle between the Z' axis and the line joining the center of the arc to the origin. The centres for the arcs for θ = 10, 20, 30 and 40^0 in the figure are at (0.5,-0.009), (0.5,-0.182), (0.5,-0.289), (0.5,-0.419) respectively, (c) Plot of Y"/(1/R) vs Y'/(1/R) (d) Plot of M"/ (C_0/A_0) vs M' / (C_0/A_0) (e) Plot of ε"/ (A_0/C_0) vs ε' / (A_0/C_0) . Values used for calculations are R=5 KΩ, A_0=6.014*10^{-6} and C_0=1.6*10^{-12} F

It can be shown that Z' and Z" satisfy the equation

4.3.2 Model 2 : Series combination of R and CPE

A series combination of resistance R and Constant Phase angle Element (CPE) is shown schematically in Figure 4.3(a). The expressions for real and imaginary parts of Z*, M*, Y* and ε * for the above model are given in Equations (4.19-4.26)

$$Z^* = R + [A_0(j\omega)^{\Psi}]^{-1} \quad Z' = R + \frac{1}{A_0\ \omega^{\Psi}} \cos\left(\frac{\Psi\pi}{2}\right), \quad Z'' = \frac{1}{A_0\ \omega^{\Psi}} \sin\left(\frac{\Psi\pi}{2}\right) \tag{4.19}$$

$$M' = \omega C_0 \quad Z'' = \omega C_0 \left(\frac{1}{A_0\ \omega^{\Psi}} \sin\left(\frac{\Psi\pi}{2}\right) \right. \tag{4.20}$$

$$M'' = \omega C_0 \quad Z' = \omega C_0 \left(R + \frac{1}{A_0\ \omega^{\Psi}} \cos\left(\frac{\Psi\pi}{2}\right) \right) \tag{4.21}$$

$$Y' = Z' / (Z'^{\,2} + Z''^{\,2}) = \frac{R + \frac{1}{A_0\ \omega^{\Psi}} \cos\left(\frac{\Psi\pi}{2}\right)}{\left(R + \frac{1}{A_0\ \omega^{\Psi}} \cos\left(\frac{\Psi\pi}{2}\right)\right)^3 + \left(\frac{1}{A_0\ \omega^{\Psi}} \sin\left(\frac{\Psi\pi}{2}\right)\right)^2} \tag{4.22}$$

$$Y'' = Z'' / (Z'^{\,2} + Z''^{\,2}) = \frac{\frac{1}{A_0\ \omega^{\Psi}} \sin\left(\frac{\Psi\pi}{2}\right)}{\left(R + \frac{1}{A_0\ \omega^{\Psi}} \cos\left(\frac{\Psi\pi}{2}\right)\right)^3 + \left(\frac{1}{A_0\ \omega^{\Psi}} \sin\left(\frac{\Psi\pi}{2}\right)\right)^2} \tag{4.23}$$

$$\varepsilon' = Y'' / (\omega C_0) \ , \varepsilon'' = Y' / (\omega C_0) \tag{4.24}$$

It can be shown that Z' , Z'' , Y' and Y'' satisfy the following equations

$$Z'' = Z' \tan\left(\frac{\Psi\pi}{2}\right) - R \tan\left(\frac{\Psi\pi}{2}\right) \tag{4.25}$$

$$\left(Y' - \frac{1}{2R}\right)^2 + \left(Y'' + \frac{1}{2R} \cot\left(\frac{\Psi\pi}{2}\right) \right)^2 = \left(\frac{1}{2R}\right)^2 \left(1 + \cot^2\left(\frac{\Psi\pi}{2}\right)\right) \tag{4.26}$$

Equation (4.25) indicates that Z'' vs. Z' plot would be a straight line with intercept with Z' axis at the point (R,0) and slope $\tan\left(\frac{\Psi\pi}{2}\right)$. It means that if we get a linear pattern in the Z'' vs. Z' plot a CPE connected in series may be used in the model. The values of Ψ and R are obtained from the slope of the straight line and the intercept on the Z' axis. Equation (4.26) indicates that Y'' vs. Y' plot is a semicircular arc with center at the point $\left(\frac{1}{2R}, -\frac{1}{2R}\cot\left(\frac{\Psi\pi}{2}\right)\right)$ below the Y' axis and radius equal to $\left(\frac{1}{2R}\sqrt{1 + \cot^2\left(\frac{\Psi\pi}{2}\right)}\right)$. This arc intercepts the Y' axis at the point $\left(\frac{1}{2R}, 0\right)$.

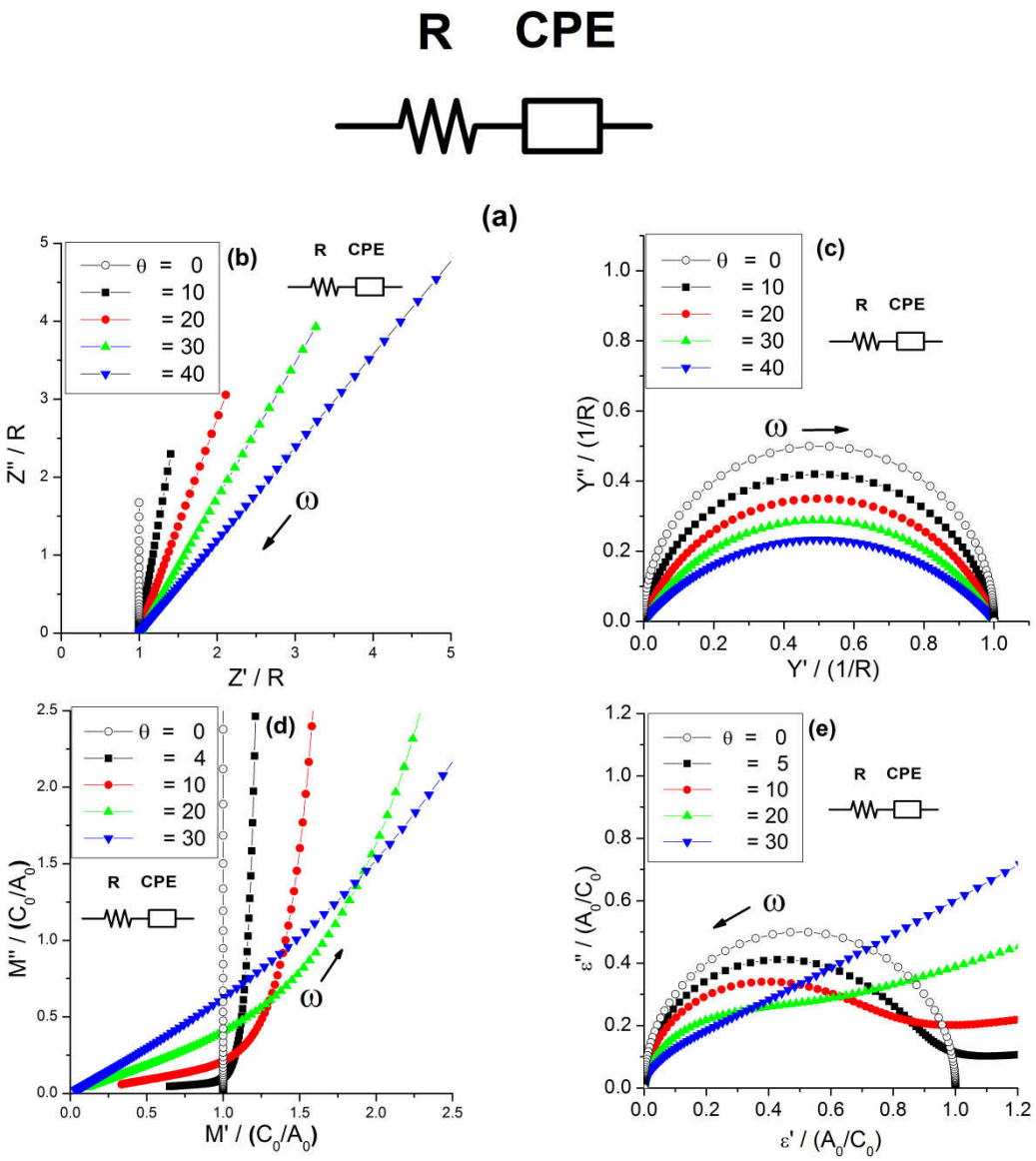

Figure 4.3 : (a) Equivalent Circuit Model containing a series combination of resistance R and CPE. (b) Z"/R vs Z'/R plots (c) Y"R vs Y'R plots (d) M"/(C_0/A_0) vs M'/(C_0/A_0) plots (e) ε"/(A_0/C_0) vs ε"/(A_0/C_0) plots for various values of parameters. Values used for calculations are R=5 KΩ,A_0=6.014*10^{-6} and C_0=1.6*10^{-12}F.

If θ is the angle between the Y′ axis and the line joining the center of the arc to the origin, then we get $\tan(\theta) = \cot\left(\frac{\Psi\pi}{2}\right)$ which yields $\pi/2 - \theta = \frac{\Psi\pi}{2}$ or $\Psi = 1 - \theta/(\pi/2) = 1 - \alpha$, $0 < \alpha < 1$ [Macdonald (2005)]. The values of Ψ and R may also be obtained from the coordinates of the centre of the semicircular arc representing the Y" vs Y' plot. Some simulated complex plane plots are shown in Figures 4.3(c-d). The values have

been appropriately normalized for a clear visualization. It is evident that the M and ε plots do not reveal much information and are not so much useful here.

4.3.3 Model 3 : Series combination of parallel $R_1 - CPE_1$ and parallel $R_2 - CPE_2$

A series combination of parallel $R_1 - CPE_1$ and parallel $R_2 - CPE_2$ is shown schematically in Figure 4.4(a) . The expressions for real and imaginary parts of Z* for the above model are given in Equations (4.27, 4.28)

$$Z^* = \frac{R_1}{1+ A_{01} R_1 (j\omega)^{\Psi_1}} + \frac{R_2}{1+ A_{02} R_2 (j\omega)^{\Psi_2}} \quad (4.27)$$

$$= \frac{R_1}{1+ (j\omega\tau_1)^{\Psi_1}} + \frac{R_2}{1+ (j\omega\tau_2)^{\Psi_2}} \quad (4.28)$$

where $\tau_1 = (A_{01} R_1)^{(1/\Psi 1)}$, $\Psi_1 = 1-\theta_1/(\pi/2) = 1- \alpha_1$ (4.29)

and $\tau_2 = (A_{02} R_2)^{(1/\Psi 2)}$, $\Psi_2 = 1-\theta_2/(\pi/2) = 1- \alpha_2$. (4.30)

It may be noted here that parallel R_1-CPE_1 and parallel R_2-CPE_2 connected in series would give rise to two separate depressed circular arcs when their response frequencies are widely separated. If we assume that R_1-CPE_1 responds at much higher frequencies than R_2-CPE_2, then in that case θ_1 would be the angle between Z' axis and the line joining the centre, $(R_1/2, -(R_1/2) \tan \theta_1)$, of the depressed circular arc corresponding to R_1-CPE_1 to the origin. The low frequency side intercept for this only will be at the point $(R_1, 0)$. Therefore θ_2 would be the angle between Z' axis and the line joining the centre, $(R_2/2, - (R_2/2) \tan \theta_2)$, of the depressed low frequency side circular arc corresponding to R_2-CPE_2, to the point $(R_1,0)$. The overall low frequency intercept of this combination will be at the point $(R_1 + R_2, 0)$.

The values of other immittance functions are obtained by using their inter relationship. The simulated immittance plots for this model are shown in Figures 4.4 (b-e). The values have been normalized for easy comparison. The limiting values of various immittance functions given below were used for normalization:

$$Z' = R_1+R_2 \quad \text{and } Y'= 1/(R_1+R_2) \text{ for } \omega = 0 \tag{4.31}$$

$$M' = C_0 (1/A_{01} + 1/A_{02}) \text{ for } \Psi = 1 \text{ and } \omega \rightarrow \infty \text{ and} \tag{4.32}$$

$$\varepsilon' = (C_1/C_0)\,[R_1/(R_1+R_2)]^2 + (C_2/C_0)\,[R_2/(R_1+R_2)]^2 \text{ for } \Psi = 1 \text{ and } \omega \rightarrow 0 \tag{4.33}$$

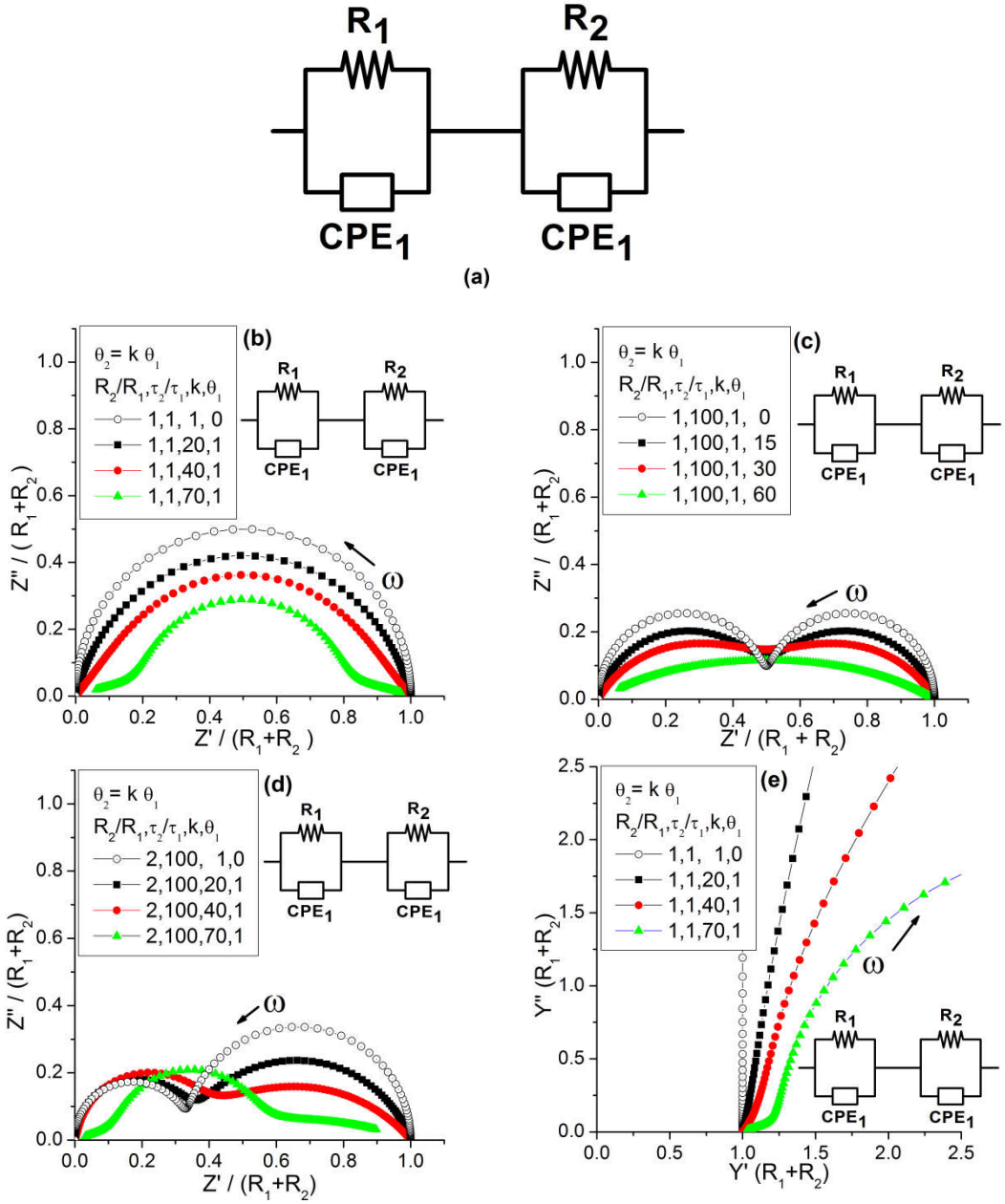

Figure 4.4 : (a) Equivalent circuit model containing series combination of parallel R_1 – CPE_1 and parallel R_2 – CPE_2 . (b-d) Plot of Z"/R vs Z'/R for various values of R_2/R_1, τ_2/τ_1 , k (θ_2=k θ_1) and θ_1 , where θ_1 is the angle between Z' axis and the line joining the origin to the centre $(\frac{R_1}{2}, -\frac{R_1}{2}\tan\theta_1)$ of the arc corresponding to the parallel combination R_1-CPE_1. θ_2 is the angle between Z' axis and the line joining the point (R_1,0) to the centre $(\frac{R_2}{2}, -\frac{R_2}{2}\tan\theta_2)$ of the arc corresponding to the parallel combination R_2-CPE_2. (e) Plots of Y"(R_1+R2) vs Y'(R_1+R_2) for various values of R_2/R_1, τ_2/τ_1 , k (θ_2=k θ_1) and θ_1 Values used for calculations are R=5 KΩ, A_{01}=6.014*10^{-6} and C_0=1.6*10^{-12} F.

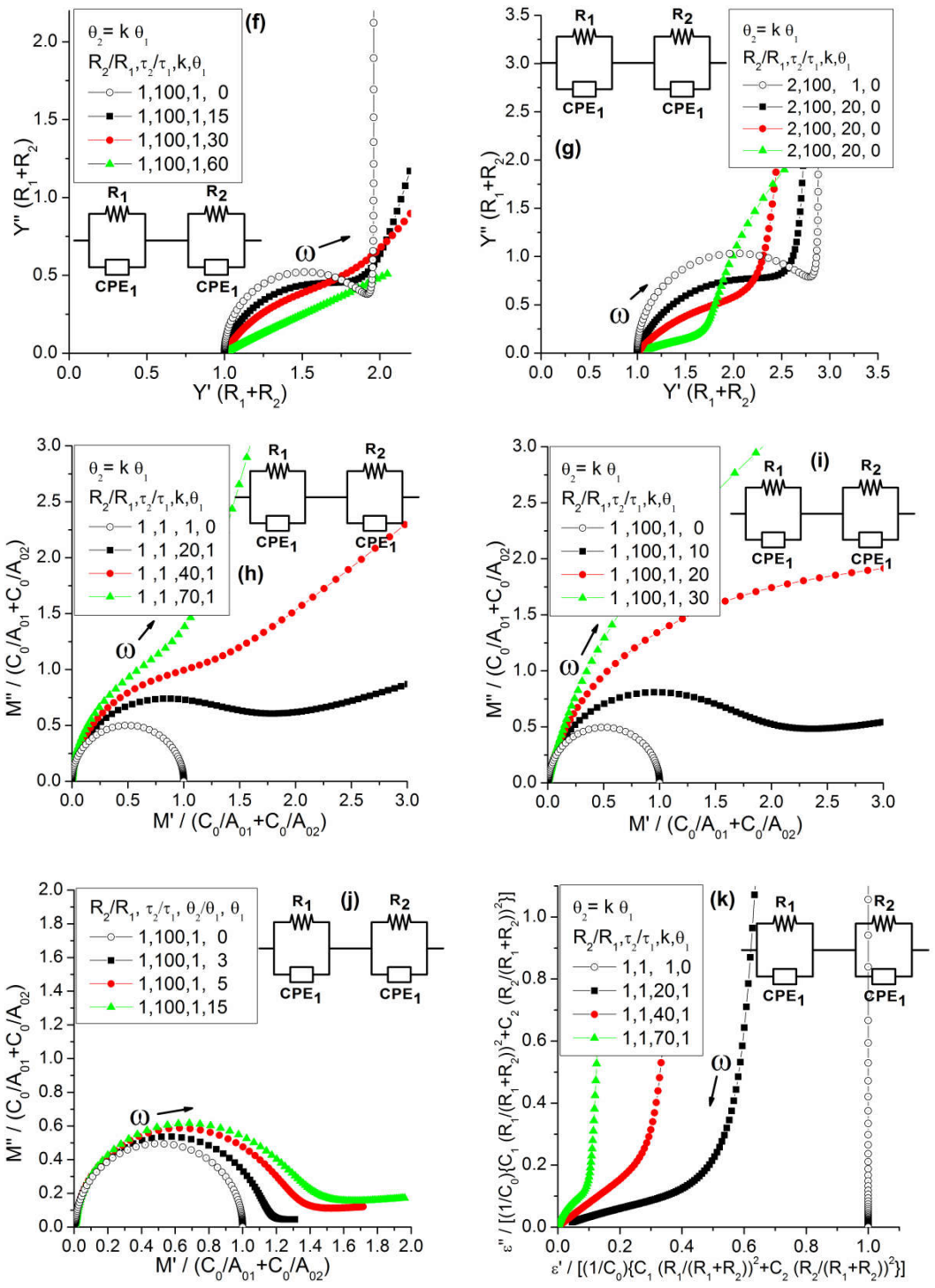

Figure 4.4 (contd.): (f-g) Plots of Y"(R_1+R2) vs. Y'(R_1+R_2) for various values of R_2/R_1, τ_2/τ_1, k (θ_2=k θ_1) and θ_1, (h-j) Plots of M"/(C_0/A_{01} + C_0/A_{02}) vs. M'/(C_0/A_{01} + C_0/A_{02}) for various values of R_2/R_1, τ_2/τ_1, k (θ_2=k θ_1) and θ_1. (k) Plot of $\varepsilon''/[(1/C_0)\{C_1 (R_1/(R_1+R_2))^2 + C_2 (R_2/(R_1+R_2))^2\}]$ vs. $\varepsilon'/[(1/C_0)\{C_1 (R_1/(R_1+R_2))^2 + C_2 (R_2/(R_1+R_2))^2\}]$ for various values of R_2/R_1, τ_2/τ_1, k (θ_2=k θ_1) and θ_1. Values used for calculations are R=5 KΩ, A_{01}=6.014*10^{-6} and C_0=1.6*10^{-12} F.

4.3.4 Model 4: Series combination of parallel R_1C_1, parallel R_2C_2 and CPE

A series combination of parallel R_1C_1, parallel R_2C_2 and CPE is shown schematically in Figure 4.5 (a). The expressions for real and imaginary parts of Z* for the above model are given in Equations (4.34, 4.35).

$$Z' = \frac{R_1}{1+(\omega C_1 R_1)^2} + \frac{R_2}{1+(\omega C_2 R_2)^2} + \left(\frac{1}{A_0\,\omega^{\psi}}\right)\cos\left(\frac{\psi\pi}{2}\right) \qquad (4.34)$$

$$Z'' = \frac{\omega C_1 R_1 R_1}{1+(\omega C_1 R_1)^2} + \frac{\omega C_2 R_2 R_2}{1+(\omega C_2 R_2)^2} + \left(\frac{1}{A_0\,\omega^{\psi}}\right)\sin\left(\frac{\psi\pi}{2}\right) \qquad (4.35)$$

The values of other immittance functions are obtained by using inter relations. The simulated immittance plots for this model are shown in Figure 4.5(b-m). The values have been suitably normalized for easy comparison.

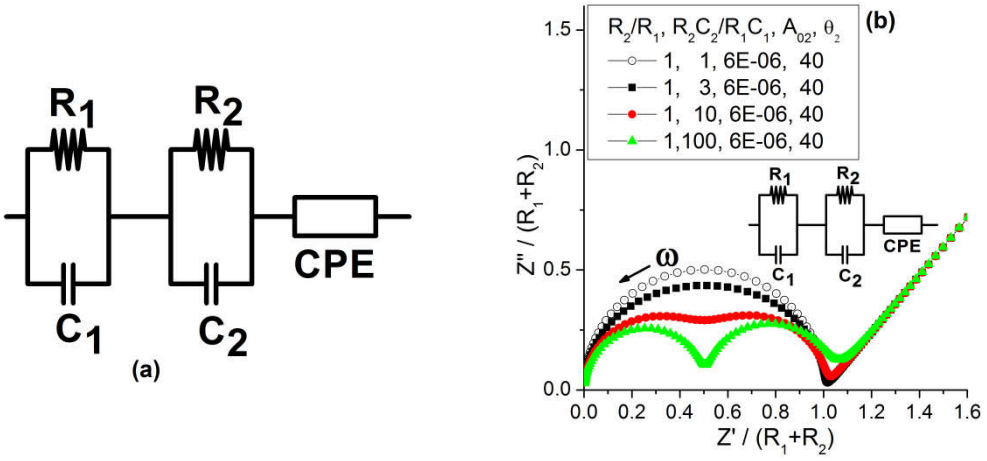

Figure 4.5: (a) Equivalent circuit model containing series combination of parallel R_1C_1, parallel R_2C_2 and CPE . Plots of (b) Z''/(R_1+R_2) vs Z'/(R_1+R_2) for various values of R_2/R_1, R_2C_2/R_1C_1, A_0 and θ , where θ is the angle between Z' axis and the line showing the low frequency linear part corresponding to CPE and passing through the point (R_1+R_2, 0) for various values of R_2/R_1, R_2C_2/R_1C_1, A_0 and θ .

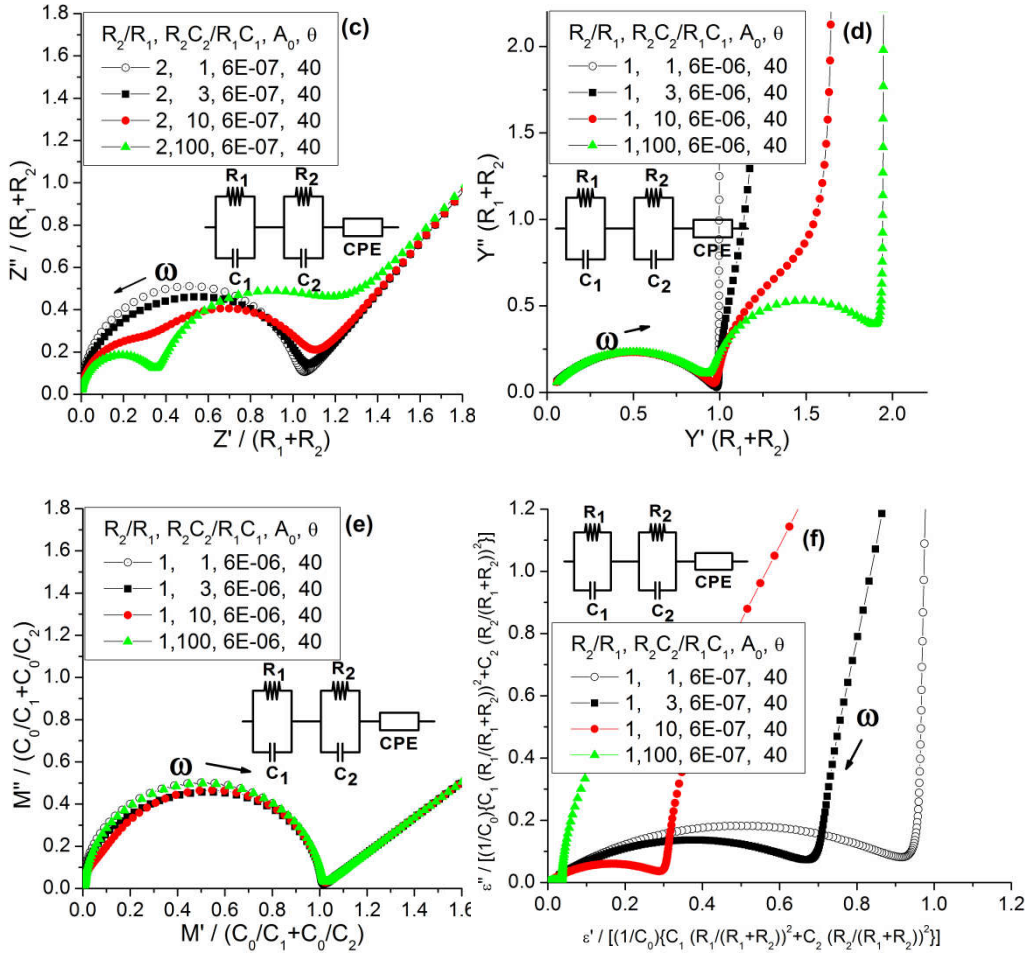

Figure 4.5 (contd.) : (c) $Z''/(R_1+R_2)$ vs $Z'/(R_1+R_2)$ for various values of R_2/R_1, R_2C_2/R_1C_1, A_0 and θ , where θ is the angle between Z' axis and the line showing the low frequency linear part corresponding to CPE and passing through the point $(R_1+R_2, 0)$ (d) $Y''(R_1+R_2)$ vs $Y'(R_1+R_2)$, (e) $M''/(C_0/C_1+C_0/C_2)$ vs $M'/(C_0/C_1+C_0/C_2)$ and (f) $\varepsilon''/[(1/C_0)\{C_1(R_1/(R_1+R_2))^2+C_2(R_2/(R_1+R_2))^2\}]$ vs $\varepsilon'/[(1/C_0)\{C_1(R_1/(R_1+R_2))^2+C_2(R_2/(R_1+R_2))^2\}]$ for various values of R_2/R_1, R_2C_2/R_1C_1, A_0 and θ .

4.3.5 Model 5: Series combination of Parallel R_1-CPE_1, R_2 and CPE_2

A series combination of parallel R_1-CPE_1, R_2 and CPE_2 is shown schematically in Figure 4.6(a).The expressions for real and imaginary parts of Z* for the above model obtained using Equations (4.12, 4.22) are given in Equations (4.36 - 4.38) . We have

$$Z^* = \frac{R_1}{1+ A_{01}R_1 \ (j\,\omega)^{\Psi_1}} + R_2 + \frac{1}{A_{02}\ (j\omega)^{\Psi_2}} \qquad (4.36)$$

which yields

$$Z' = \frac{R_1\,(1+A_{01}\,R_1\,\omega^{\Psi_1}\cos(\frac{\Psi_1\ \pi}{2})}{(1+A_{01}\,R_1\,\omega^{\Psi_1}\cos(\frac{\Psi_1\ \pi}{2})^2\ +(A_{01}\,R_1\,\omega^{\Psi_1}\sin(\frac{\Psi_1\ \pi}{2})^2} + R_2 + \frac{1}{A_{02}\ \omega^{\Psi_2}}\cos(\frac{\psi_2\,\pi}{2}) \quad (4.37)$$

$$Z'' = \frac{R_1\,(A_{01}\,R_1\,\omega^{\Psi_1}\sin(\frac{\Psi_1\ \pi}{2})}{(1+A_{01}\,R_1\,\omega^{\Psi_1}\cos(\frac{\Psi_1\ \pi}{2})^2\ +(A_{01}\,R_1\,\omega^{\Psi_1}\sin(\frac{\Psi_1\ \pi}{2})^2} + \frac{1}{A_{02}\ \omega^{\Psi_3}}\sin(\frac{\psi_2\,\pi}{2}) \quad (4.38)$$

Expressions for other immittance functions may be derived by using these. For calculations we have let $A_{01}R_1 = \tau_1^{\Psi_1}$ and $A_{02}R_2 = \tau_2^{\Psi_2}$ [Macdonald et al. (2005)]. Complex plane plots of various immittance functions are shown in Figures 4.6 (b-i) for different values of the parameters. Values used for calculations are R_1=5 KΩ, A_{01} = $2*10^{-11}$. For simple visualization of the plots we may remember that if $\tau_1 << \tau_2$ i.e. parallel R_1-CPE_1 responds at much higher frequencies than the series R_2-CPE_2 then the higher frequency portion of the Z" vs Z' plot (i.e. the left hand side portion) would be a depressed semicircular arc having highest frequency intercept with the Z' axis at the point (R_2, 0) and centre at (R_2 +0.5 R_1, - 0.5 R_1tan θ_1). The possible lower frequency intercept would be at the point (R_2+R_1, 0). The angle θ_1 (=(1-Ψ_1)π/2) is the angle between Z' axis and the line joining the point (R_2, 0) to the centre (R_2 +0.5 R_1, - 0.5 R_1 tan θ_1). The low frequency side (i.e. right hand side portion) of the Z" vs. Z' plot, representing the series R_2-CPE_2 segment, would be a straight line passing through the point (R_1+R_2,0) and making an angle θ_2 with the Z' axis. The corresponding Y" vs. Y' plots would have these rolls reversed and the plot would traverse from left side towards right side as the frequency is raised. The low frequency portion, corresponding to the R_2-CPE_2 segment, would now be a depressed semicircular arc with centre at (0.5 R_2, - 0.5 R_2 cot (Ψ_2 π/2).

. The angle between Y' axis and the line joining this centre to the origin would be $\theta'_2 = (1 - \Psi_2)$ $\pi/2 = \pi/2 - \theta_2$. The high frequency portion would be a straight line making an angle $\theta'_1 = \Psi_1 \pi/2$ $= \pi/2 - \theta_1$.

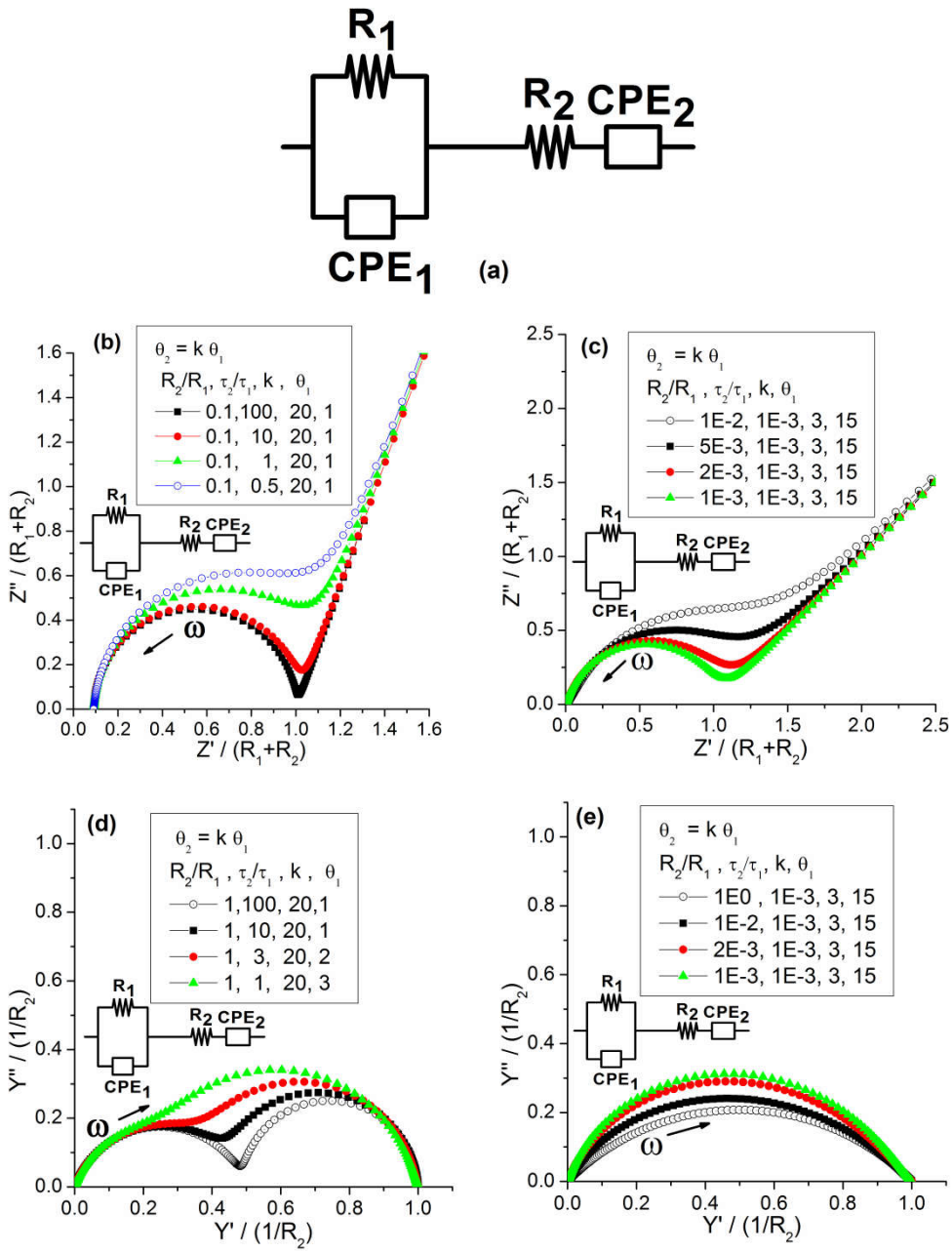

Figure 4.6 :(a) Equivalent circuit model having series combination of parallel R_1-CPE_1 , R_2 and CPE_2 .(b,c) Plot of $Z''/(R_1+R_2)$ vs $Z'/(R_1+R_2)$ for various values of R_2/R_1, τ_2/τ_1, θ_2/θ_1 and θ_1 . where θ_1 is the angle between Z' axis and the line joining the highest frequency intercept point $(R_2,0)$ to the point ($R_2+0.5R_1$, $- 0.5R_1 \tan \theta_1$), the center of the semi circular arc corresponding to parallel R_1-CPE_1 . (d-e) Plot of $Y''/(1/R_2)$ vs $Y'/(1/R_2)$.

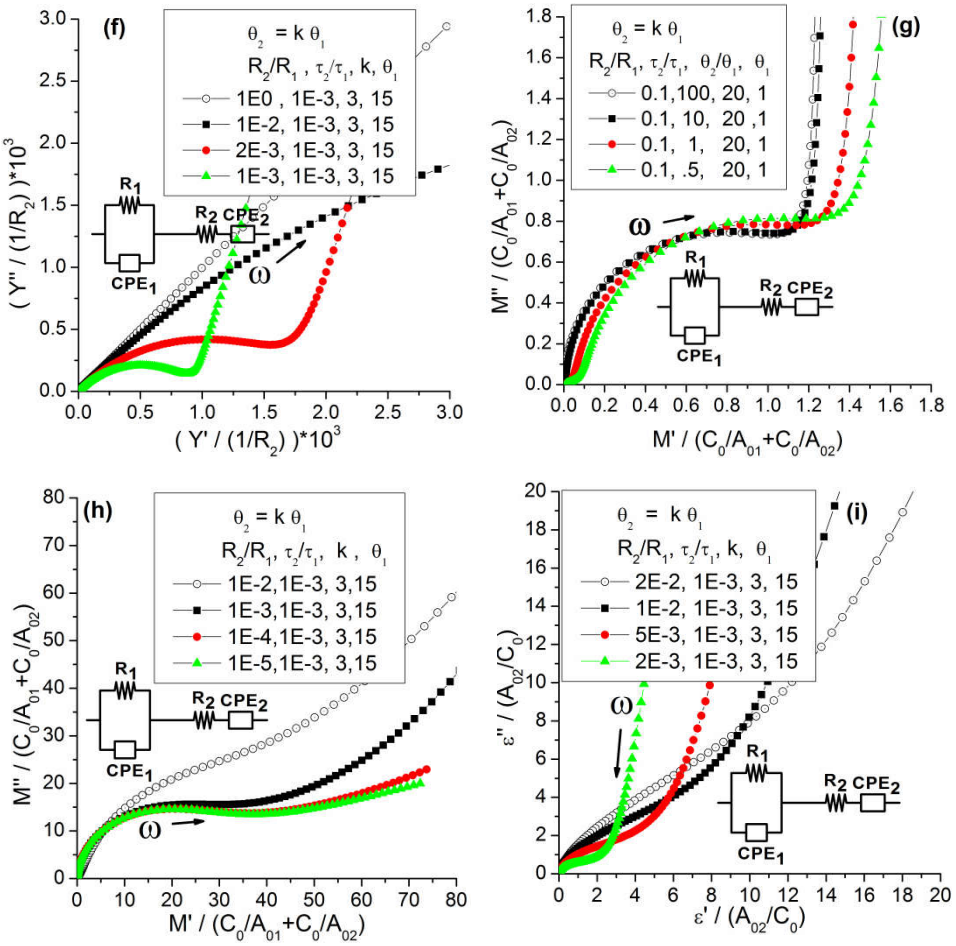

Figure 4.6(contd.): (f) Plot of $Y''/(1/R_2)$ vs $Y'/(1/R_2)$. (g,h) Plot of $M''/(C_0/A_{01}+C_0/A_{02})$ vs $M'/(C_0/A_{01}+C_0/A_{02})$. (i) Plot of $\varepsilon''/(A_{02}/C_0)$ vs $\varepsilon'/(A_{02}/C_0)$.

4.3.6 Model 6: Parallel combination R_2C_2 in series with parallel combination of and R_1 ,C_1 and CPE_1

A Parallel combination R_2C_2 connected in series with parallel combination of and R_1 ,C_1 and CPE_1 is shown schematically in Figures 4.7 (a) . The expressions for real and imaginary parts of Z^* for the above model obtained using Equations (4.11, 4.12, 4.14) are given in Equations (4.39 and 4.40) .

$$Z' = \frac{R_1\,(1+\ R_1\ A_{01}\,\omega^{\Psi_1}\cos(\frac{\Psi_1\ \pi}{2})}{(1+\ R_1\ A_{01}\,\omega^{\Psi_1}\cos(\frac{\Psi_1\ \pi}{2})^2\ +(\ R_1\ A_{01}\,\omega^{\Psi_1}\sin(\frac{\Psi_1\ \pi}{2})^2} + \frac{R_2}{1+(\omega\,C_2\,R_2)^2} \qquad (4.39)$$

$$Z'' = \frac{R_1\,[\,(R_1\ A_{01}\,\omega^{\Psi_1}\sin\left(\frac{\Psi_1\ \pi}{2}\right) + \omega\,C_1\,R_1]}{(1+A_{01}\,R_1\,\omega^{\Psi_1}\cos(\frac{\Psi_1\ \pi}{2})^2\ +(A_{01}\,R_1\,\omega^{\Psi_1}\sin(\frac{\Psi_1\ \pi}{2})^2} + \frac{R_2\ \omega\,C_2\,R_2}{1+(\omega\,C_2\,R_2)^2} \qquad (4.40)$$

Expressions for other immittance functions may be derived by using these. The simulated immittance plots for this model for various ratios of the components are shown in Figures 4.7 (b-j). The values of some of the components used are R_1= 5 K Ohm, C_1=20 pF, C_0=1.6pF. For easy comparison suitably normalized values have been plotted as labeled on the axes and are given below

$Z' = R_1+R_2$ and $Y'= 1/(R_1+R_2)$ for $\omega = 0$ and $\Psi = 1$,

$M'= C_0/C_1 + C_0/C_2$ for $\omega \rightarrow \infty$ (4.41)

$\varepsilon' = (C_1/ C_0) [R_1 /(R_1+R_2)]^2 + (C_2/ C_0) [R_2/(R_1+R_2)]^2$ for $\Psi = 1$ and $\omega \rightarrow 0$ (4.42)

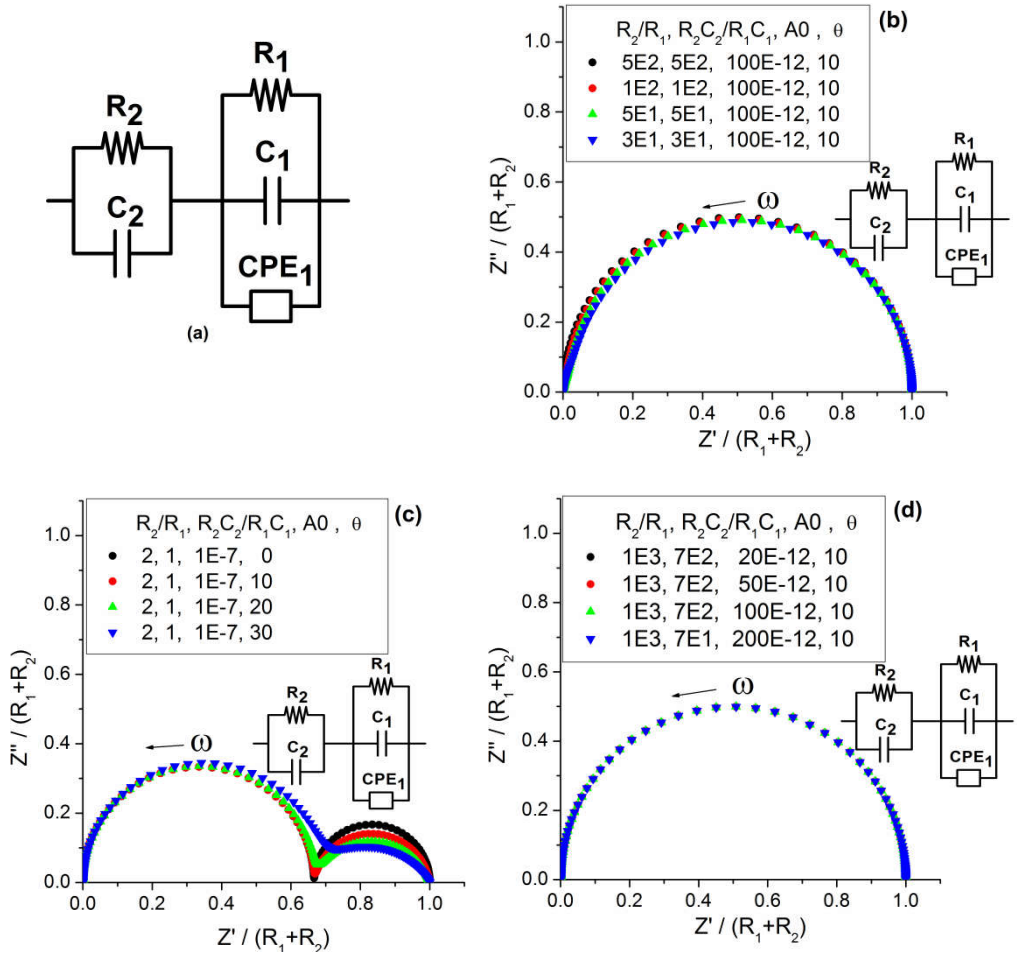

Figure 4.7: (a) Equivalent circuit model having a parallel combination R_2C_2 connected in series with parallel combination of and R_1-C_1 and CPE_1 . Plots of (b-d) $Z''/(R_1+R_2)$ vs $Z'/(R_1+R_2)$ for various values of R_2/R_1, R_2C_2/R_1C_1, A_0 and θ for various values of R_2/R_1, R_2C_2/R_1C_1, A_0 and θ .

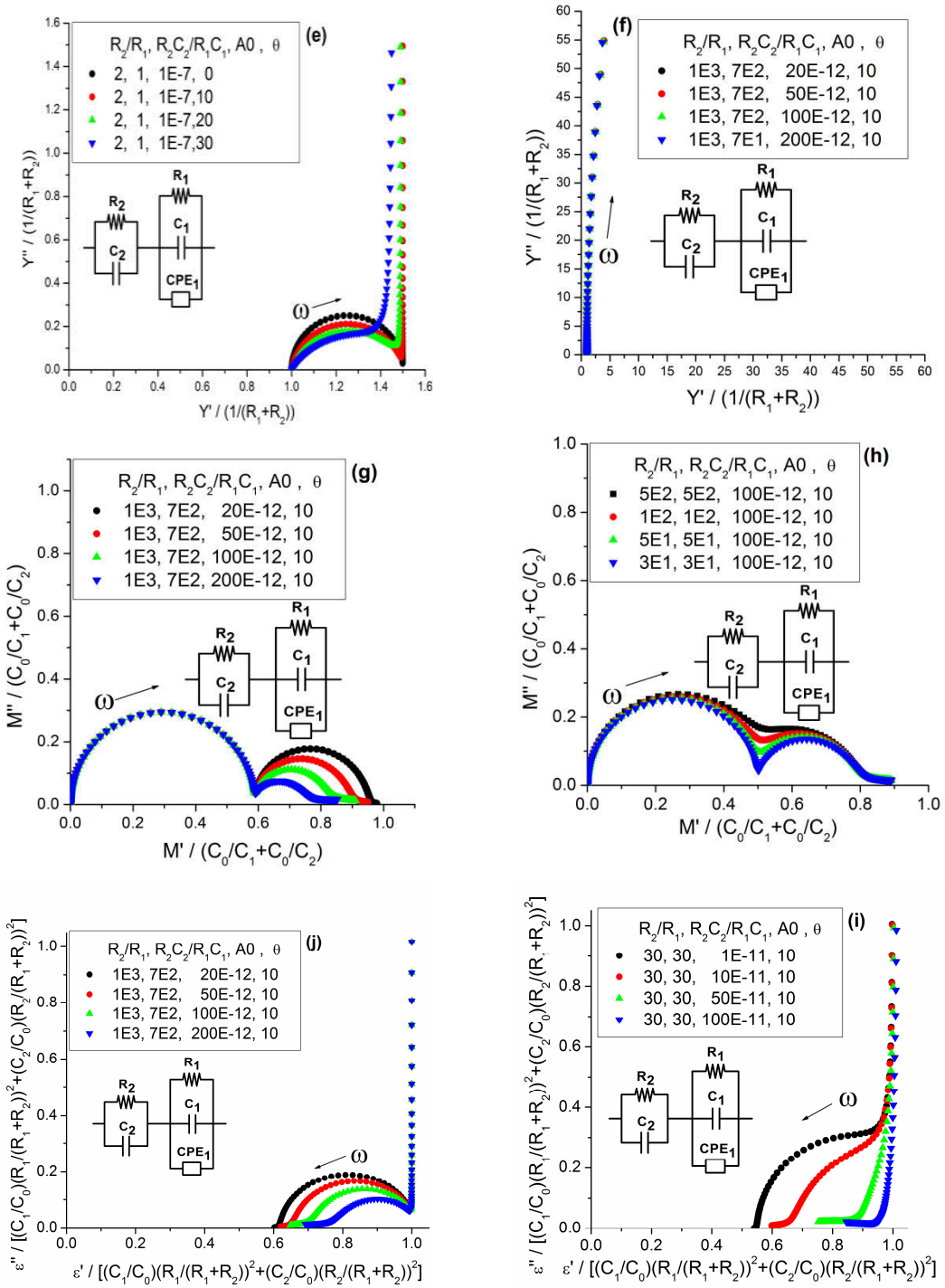

Figure 4.7 (contd.) : Plots of (e-f) Y”(R_1+R_2) vs Y’(R_1+R_2) , (g,h) M”/(C_0/C_1+C_0/C_2) vs M’/(C_0/C_1+C_0/C_2) and (i-j) ε”/[(C_1/C_0)(R_1/(R_1+R_2))^2+(C_2/C_0)(R_2/(R_1+R_2))^2] vs ε’/[(C_1/C_0)(R_1/(R_1+R_2))^2+(C_2/C_0)(R_2/(R_1+R_2))^2] for various values of R_2/R_1, R_2C_2/R_1C_1, A_0 and θ .

4.4 Discussion

From the figures shown in section 3 it is clear that different combinations of CPE will show different immittance plots. Some immittance plots for various RC combinations , RL combinations and RLC combinations have been given earlier [Macdonald. (2005), Pandey et al. (1995); Katare et al. (1999); Chaitanya et al. (2011)]. By comparing the experimentally observed plots with those presented in this chapter and in the references given above, one can arrive at a guess about a possible equivalent circuit model that might be used to represent the impedance behavior of the material. The plots shown in this chapter would be useful when the immittance plots possess depressed arcs or linear portions in complex plane. The choice of an equivalent circuit model is a difficult process becoming more so as several equivalent circuits may yield the same frequency dependence of the impedance [Macdonald (2005), Pandey et al. (1995);]. However a clue can be obtained by looking at the experimental plots for various conditions viz temperature, composition and microstructure and comparing them with the simulated plots given in this chapter for various models. It is always desirable to select the simple possible model to start with [Sinclair et al. (1994)].

As an example we consider the Model 3 having two parallel R-CPE connected in series. The Z'' vs Z' plots contain well resolved semicircular type depressed arcs when the time constants are well separated, but show a hump when the time constants are close to each other. However, the M" vs M' plots show a hump and a flattening trend at high frequency side. The Y" vs Y' and ε'' vs ε' plots do not provide much information. Thus in an experimental measurement , a flattened type high frequency trend in M" vs M' plot and depressed arc(s) in Z" vs Z' plot would indicate that a parallel R-CPE combination connected in series with another R-CPE might be a

suitable model to be used to represent the data. We now look at Model 4 that contains two parallel RC's connected in series with a CPE . Both the Z" vs Z' and M" vs M' plots possess a linear portion together with overlapping or resolved arcs.

An experimental plot showing a linear portion in the complex plane plot of this type would indicate that the equivalent circuit would involve a CPE connected in series and the circuit given in Model 4 might be useful to start with. This model has been used earlier also [Katare et al. (2003)] but details of other immittance plots were not given. Similarly, we look at Model 5 which contains a parallel R-CPE, a resistance and a CPE all connected in series. The Z" vs Z' plots show a shift (corresponding to R_2), an arc (owing to parallel R_1-CPE_1) and a linear portion (arising due to CPE_2). The Y" vs Y' plots show overlapping or resolved arcs depending upon the ratios of the components. Now let us consider Model 6. A model comprising series combination of a capacitor and CPE connected in parallel to another capacitor and a resistance was proposed [Macdonald (2005)] and used [Casiola et al.(1983)] for representing depressed arcs. In order to simulate complex plane plots having a semicircular arc connected to a depressed arc a simplified circuit shown in Figure 4.7 (a) was developed. The Z" vs Z' plot may be a single arc, well resolved arcs or overlapping arcs or one semicircular arc connected to depressed arc as shown in Figures 4.7 (b-d) depending upon the ratios of the components. Similar behavior is seen in the M" vs. M' plots shown in Figures 4.7 (g,h).

As an illustration, an analysis of the room temperature impedance data obtained for the system $Ba_{1-x}Sr_xTiO_3$ (x = 0.35) is now presented. The impedance measurements were carried out at room temperature in the frequency range from 0.01 Hz to 1 MHz. It may be mentioned that the system $Ba_{1-x}Sr_xTiO_3$ is a ferroelectric for which the ferroelectric to paraelectric phase transition temperature T_c shifts towards lower temperatures as x is increased. For x = 0.35 , T_c is close to room temperature. The preparation and characterization of this system is described in detail in Chapter 5, where models representing the behavior above T_c are discussed. In what follows we develop an equivalent circuit model that represents the data well.

It is known that analysis of the data by using only one immittance formalism does not suffice and at least two formalisms should be looked at [Pandey et al. (1995)]. We choose to consider Z and M data. Figure 4.8 (a) shows Z' and Z'' vs $\log_{10}(f)$ plot and Figure 4.8 (b) shows Z" vs Z' plot for this system at 303 K. Similarly Figure 4.8 (c) shows M' and M'' vs $\log_{10}(f)$ and Figure 4.8 (d) M" vs M' plots. The values of M' and M'' were derived from the Z data by using the relations $M' = \omega C_0 Z''$ and $M'' = \omega C_0 Z'$ where $C_0 = 8.1697*10^{-12}$ F. As there is no steeply rising high frequency branch in the M" vs M' plot and no shift in the corresponding Z" vs Z' plot , presence of series resistance in the model is ruled out. Similarly there is no shift in M" vs M' plot indicating that there is no series capacitance in the model. Also there are no linear portions in the M" vs M' or Z" vs Z' plots indicating that the model would not contain any series CPE. The M" vs M' plot in Figures 4.8 (d) has two arcs where the one at low frequency side (at the left side of the plot) is almost semicircular and the other at higher frequency side (at the right hand side of the plot) is depressed . Had there been two

clear well separated semicircular arcs , a model comprising two parallel RC circuits in series would have been useful. Here we have one almost clear semicircular arc and the other a depressed one.

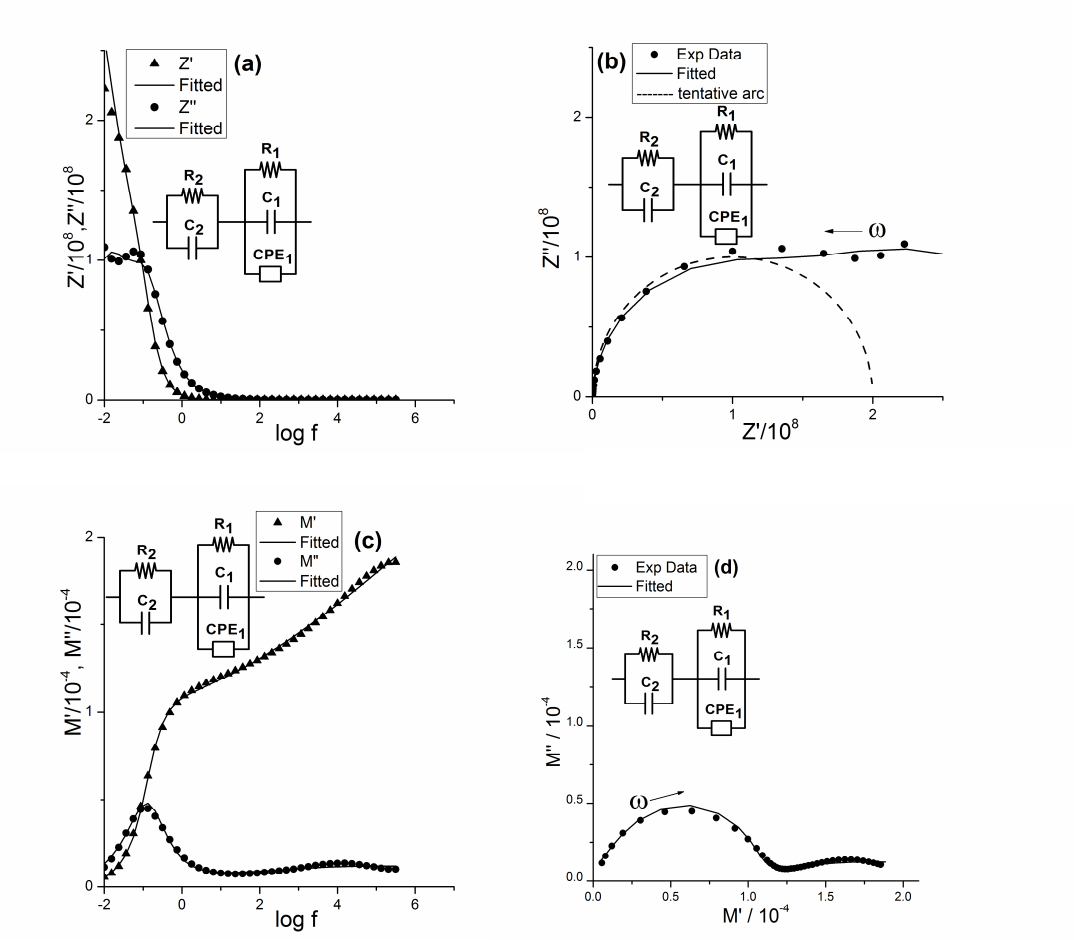

Figure 4.8 : Experimental and fitted values of (a) Z″, Z′ vs. log f, (b) Z″ vs. Z′, (c) M″, M′ vs. log and (d) M″ vs. M′ for ceramic system $Ba_{1-x}Sr_xTiO_3$ (x=0.35) by using the model shown in Figure 4.7(a).

Keeping in mind that a CPE connected in parallel produces a depressed arc in M" vs. M' plot [Macdonald (2005); Casciola (1983)] and comparing the experimental plot with simulated ones given in section 3, it is seen that the model circuit needed to represent this system would be similar to the one shown in Figure 4.7(a) i.e. a parallel R_2C_2 in series with a parallel R_1C_1 which is shunted by a CPE_1. As the Z" vs. Z' plot of Figure 4.8(b) is almost a single arc , it is inferred that R_2C_2 is much larger than R_1C_1 .The values of the components are now estimated. From the low frequency intercept of

a tentative semicircular arc in the Z" vs Z' plot (Figure 4.8 (b)) we assume $R_2 \sim 2*10^8$ Ohms and from this we get $C_2 \sim 5.4*10^{-9}$ F by using $\omega C_2 R_2=1$. Looking at the simulated M" vs. M' plots of Figure 4.7 (g,h) C_1 is chosen approximately equal to C_2 ie $C_1 \sim 3*10^{-9}$ F and $A_{01} \sim 10*C_2 \sim 5.6*10^{-8}$. Again by comparing the plot of Figure 4.8 (d) with the simulated plot of Figure 4.7 (g, h), we assume $\theta \sim 10$ degrees ie $\psi = 1-\theta/90 \sim 0.89$.

From the high frequency curve of the M" vs. M' plot (Figure 4.8(d)) we assume $R_1 \sim 3445$ Ohms. The values of the parameters were determined more accurately by using CNLS program IMPSPEC.BAS being regularly used in our laboratory [Chaitanya et al. (2015); Chaitanya et al. (2011); Pandey et al. (1997); Pandey (1992)] and using the above mentioned values as initial guesses. The values thus obtained are $R_1 = (2.31 \pm 0.17)*10^8$ Ohms, $A_{01} = (3.53 \pm 0.05)*10^{-8}$, $C_1 = (4.16 \pm 0.08)*10^{-9}$ F, $R_2 = (1.30 \pm 0.03)*10^8$ Ohm $C_2 = (9.83 \pm 0.07)*10^{-9}$ F and $\psi = 0.842 \pm 0.002$. Figure 4.8 shows experimental as well fitted data in the Z and M plots. The overall impedance behavior of a polycrystalline ceramic would stem from grain, grain boundary and electrode contributions generally represented by three parallel RC's connected in series . The lowest frequency response is usually attributed to the electrode process and the high frequency to grains . From the equivalent circuit developed above, it seems that the grain and grain boundary contributions represented by combination of R_1, C_1 and CPE_1 are engulfed together.

4.5 Conclusions

Complex plane plots for Impedance Z, Modulus M, Admittance Y, Permittivity ε for equivalent circuit models involving constant phase angle elements (CPE) have

been simulated for different ratios of the parameters. A linear portion appearing in the complex plane plot may be considered as a signature of presence of series CPE in the model whereas a depressed arc in the Z" vs Z' or M" vs M' plot would indicate the presence of CPE connected in parallel. The experimental data for the ceramic system $Ba_{1-x}Sr_xTiO_3$ (x=0.35) have been analyzed in the light of these models and an equivalent circuit model representing the data is obtained. The equivalent circuit model comprises a parallel combination R_2C_2 in series with parallel combination of and R_1 , C_1 and CPE_1.The details of how to arrive at this model is also elaborated.